Polypropylene microplastic exposure leads to lung inflammation through p38-mediated NF- κB pathway due to mitochondrial damage

Jong-Hwan Woo
Korea Institute of Toxicology
Hyeon Jin Seo
Korea Institute of Toxicology
Jun-Young Lee
Korea Institute of Toxicology
Iljung Lee
Korea Radioisotope Center for Pharmaceuticals, Korea Radiological and Medical Sciences
Kisoo Jeon
VITALS Co., Ltd
Bumseok Kim
Jeonbuk National University
Kyuhong Lee (khleekit@gmail.com)
Korea Institute of Toxicology

Research Article

Keywords: Polypropylene (PP), Microparticles, Mitochondrial damage, p38, NF-κB

Posted Date: July 8th, 2022

DOI: https://doi.org/10.21203/rs.3.rs-1801803/v1

Additional Declarations: No competing interests reported.

Version of Record: A version of this preprint was published at Particle and Fibre Toxicology on January 10th, 2023. See the published version at https://doi.org/10.1186/s12989-022-00512-8.

Abstract

Background: Polypropylene (PP) is used in various products such as disposable containers, spoons, and automobile parts. The disposable masks used for COVID-19 prevention mainly comprise PP, and the disposal of such masks is concerning because of the potential environmental pollution. Recent reports have suggested that weathered PP microparticles can be inhaled, however, the inhalation toxicology of PP microparticles is poorly understood.

Results: Inflammatory cell numbers, reactive oxygen species (ROS) production, and the levels of inflammatory cytokines and chemokines in PP-instilled mice increased in a dose-dependent manner compared to the control. Histopathological analysis of the lung tissue of PP-stimulated mice revealed lung injuries, including the infiltration of inflammatory cells into the perivascular/parenchymal space, alveolar epithelial hyperplasia, and foamy macrophage aggregates. The *in vitro* study indicated that PP stimulation causes mitochondrial dysfunction including mitochondrial depolarization and decreased adenosine triphosphate (ATP) levels. PP stimulation led to cytotoxicity, ROS production, increase of inflammatory cytokines, and cell deaths in A549 cells. The results showed that PP stimulation increased the p-p38 and p-NF-κB protein levels both *in vivo* and *in vitro*, while p-ERK and p-JNK remained unchanged. Interestingly, the cytotoxicity that was induced by PP exposure was regulated by p38 and ROS inhibition in A549 cells.

Conclusions: These results suggest that PP stimulation may contribute to inflammation pathogenesis via the p38 phosphorylation-mediated NF-κB pathway as a result of mitochondrial damage.

1. Background

Worldwide, plastics are used in various products, such as face masks, disposable products, plumbing, toys, and automobile parts [1, 2]. As the use of plastics has increased, the possibility of exposure to plastics by the human body has also increased. Recent reports have suggested that various microplastics, such as polypropylene (PP), polystyrene (PS), and polyethylene terephthalate (PET) have been detected in the atmosphere as a result of physical force, hydrolysis, and ultraviolet radiation [3–6]. As the COVID-19 virus response continues, the increase in the use of disposable masks that mainly comprise PP is raising concerns about the adverse effects in humans caused by inhalation exposure to airborne weathered PP microplastics [7–9]. According to recent studies, microplastics such as PP, polyethylene (PE), and PET have been detected in the lung tissue of live humans, with PP microplastics (particles and fibre form) being the most dominant (23%) [10]. Other studies have reported the detection of polymer-type PP microplastics in human lung tissue [11]. Recent studies have reported that airborne PP microplastics accumulated in lung tissue upon inhalation [9–12], however, the toxic effects of PP microparticles in the respiratory system remain poorly understood.

Microplastics, plastics that have become micronized by weathering and sunlight, are able to easily infiltrate cells and tissues as a result of their small size, and the accumulation of these materials in the

organs alters the physiological processes [12, 13]. One previous study reported that microplastics that are 1–5 μm size can infiltrate the respiratory tract to reach the lung tissue via the lower airway, and that nanosized microplastics can infiltrate the alveolus [12]. Inhaled microplastic particles can be translocated by active cellular uptake, which occurs via contact with the bronchial epithelium after penetration of the lung lining fluid occurs [3]. Nanosized plastic particles have been observed to infiltrate the pulmonary epithelial barrier and easily pass into the bloodstream [12]. Recent studies have reported that the inhalation of nanosized plastic can lead to bronchial epithelial injury as a result of epithelial barrier infiltration, leading to inflammatory response, cytotoxicity, and genotoxicity, and that long-term exposure can lead to pulmonary diseases such as asthma and pneumoconiosis [3, 4, 12, 14]. Although several studies have reported on the toxicity of microplastics, the mechanisms underlying the development of pathogenic respiratory diseases from microplastic exposure are still not completely understood.

Mitochondria play a key role in producing energy for use by cellular organelles [15]. In addition to supplying cellular energy, mitochondria are involved in cellular metabolism, including processes such as cellular differentiation, cell death, and growth [15, 16]. Mitochondrial damage is known to induce mitochondrial dysfunctions such as depolarisation of the mitochondrial membrane potential, a decrease in adenosine triphosphate (ATP) levels, and the production of reactive oxygen species (ROS), which are important factors in cellular metabolism and have been implicated in various human diseases, including asthma and pulmonary fibrosis [15–19]. Previous reports have suggested that the mitochondrial injury that results from exposure to airborne microparticles led to toxic responses such as oxidative stress, cytotoxicity, and inflammation through the mitogen-activated protein kinase (MAPK) and nuclear factor kappa B (NF-κB) signalling pathways [12, 20]. In addition, previous studies have reported that particulate matter (PM)-instilled mice showed oxidative stress and airway inflammatory responses due to MAPK and NF-κB activation [21]. The toxic mechanisms of these airborne particles have been reported in several *in vitro* and *in vivo* studies [12, 20–23], however, the mechanism by which mitochondrial injury occurs following exposure to toxic PP microplastics is unclear.

In this study, we investigated the inflammatory response by analysing the inflammatory cytokine and chemokine levels, cellular changes, and histology of PP-instilled mice. We also examined the mechanisms of cytotoxicity, oxidative stress, and the inflammatory response that result from mitochondrial damage in PP-stimulated human lung epithelial cells (A549 cells).

2. Results

2.1 PP microplastics characterization

FE-SEM confirmed that the PP microparticles were irregular in shape and 0.66 ± 0.27 μm in size (Fig. 1a). The suspension of the PP microparticles was analyzed using DSL, which indicated that the 252 nm particles were the most widely distributed (Fig. 1b). The dispersion stability of the PP microparticle suspension was measured for 1 h at 10-min intervals using a Turbiscan, which indicated that the PP

microparticles remained stably suspended in the liquid, with little change observed in the backscattering (BS) of 0.4% for 1 h (Fig. 1c).

2.2 PP induces inflammation and ROS production in the lung of mice

Toxic responses such as inflammation and ROS production were observed in the lungs of mice following PP microplastic stimulation. Our results showed that the number of total cells, macrophages, neutrophils, and lymphocytes in the bronchoalveolar lavage fluid (BALF) of the PP-instilled mice increased in a dose-dependent manner relative to the vehicle control (VC) (Fig. 2a). Additionally, the levels of inflammatory cytokines and chemokines in the BALF, including tumor necrosis factor-α (TNF-α), interleukin (IL)-1β, IL-6, monocyte chemoattractant protein-1 (MCP-1), and C-X-C motif chemokine ligand 1 (CXCL1/KC) were significantly increased in the 2.5 and/or 5 mg/kg PP intratracheal instillation groups as compared to the VC groups (Fig. 2b-f). ROS production was also increased in the lung tissue of PP-instilled mice (2.5 and 5 mg/kg) compared to the control (Fig. 2g). Histopathological analysis of the lung tissue of PP-instilled mice showed lung lesions such as inflammatory cell infiltration, alveolar epithelial hyperplasia, and foamy macrophage aggregates (Fig. 3).

2.3 PP-instilled mice regulate p38 and NF-κB activation

The MAPK and NF-κB signaling pathways are known to contribute to the regulation of apoptosis and inflammation-related gene expression [24, 25]. Our results showed that the p-p38 protein levels in the lung tissue of PP-instilled mice were significantly increased compared to those in the VC groups, while extracellular signal-regulated kinase (ERK) and c-Jun N-terminal kinase (JNK) phosphorylation remained unchanged (Fig. 4a-d). Interestingly, the increase in the p-NF-κB protein levels in the lung tissue of PP-instilled mice compared was dose-dependent (Fig. 4a, e). These results indicate that PP stimulation might contribute to the pulmonary toxic response via the MAPK and NF-κB signaling pathways.

2.4 Mitochondrial damage and dysfunction in PP-exposed human lung epithelial cells

Previous studies have reported that PM, such as ultrafine dust and PS microplastics, damages cell organelles such as mitochondria via intracellular accumulation [26, 27]. We investigated the effects of PP stimulation on mitochondrial damage and dysfunction in A549 cells, and found that the mitochondrial membrane potential (ratio of red/green) of 4 mg/ml PP-exposed A549 cells decreased significantly as compared to that of the VC (Fig. 5a-b). In addition, the ATP levels associated with mitochondrial function in PP-exposed A549 cells were dose-dependently decreased (Fig. 5c). Mitochondrial dynamic-related proteins such as dynamin-related protein 1 (DRP1), mitofusin 1 (MFN1), and mitofusin 2 (MFN2) were observed. DRP1 proteins play an important role in the division of damaged mitochondria. Confocal microscopy showed strong intracellular fluorescence intensity for DRP1 in the 4 mg/ml PP-exposed A549

cells, however, the same was not observed for TOM20 (Fig. 6a-b). Interestingly, the images showed the merging of the TOM20 and DRP1 proteins in the PP-exposed A549 cells (Fig. 6a). In addition, western blot analysis showed that the protein levels of DRP1 were dose-dependently increased in PP-exposed A549 cells, compared with that of VC (Fig. 6c-d). In contrast, the protein levels of MFN1 and MFN2 were slightly increased (Fig. 6c-d).

2.5 PP stimulation induces ROS, inflammatory response, and cell deaths in A549 cells

ROS production, inflammation, and cell death due to mitochondrial damage were measured. ROS production increased significantly in the mitochondria of 4 mg/ml PP-exposed A549 cells compared to the VC (Fig. 7a-b). In addition, the total ROS in the 4 mg/ml PP-treated A549 cells was higher than that of the VC (Fig. 7c). Our results showed that the levels of the inflammatory cytokines TNF-α, IL-1β, and IL-6 increased in the 4 mg/ml PP-exposed A549 cells as compared to the VC (Fig. 7d-e). Interestingly, the cell viability of the 4 mg/ml PP-exposed A549 cells decreased significantly as compared to that of the VC (Fig. 7f). These results indicate that PP stimulation induced ROS production, inflammation, and cell death in A549 cells as a result of mitochondrial damage.

2.6 PP stimulation induces p38-mediated NF-κB nuclear translocation

We observed the MAPK and NF-κB pathways by PP stimulation *in vitro*. Our results showed that p38 phosphorylation significantly increased in PP-exposed A549 cells, while ERK and JNK remained unchanged (Fig. 8a-d). IκB-α and NF-κB phosphorylation in the PP-stimulated A549 cells was significantly increased compared to that in VC (Fig. 8a, e, f). Moreover, PP stimulation was observed to induce the nuclear translocation of NF-κB (Fig. 8a, g).

2.7 p38 and NF-κB activation in PP-exposed A549 cells was regulated by inhibition of ROS

Our results showed that the activation of p38 and NF-κB in PP-stimulated A549 cells was significantly decreased by p38 and ROS inhibition (Fig. 9a-c). Interestingly, inhibiting p38 and ROS in PP-treated A549 cells resulted in a marked reduction in the inflammatory cytokine levels (Fig. 9a, d-f). In addition, the cell viability of PP-exposed A549 cells was recovered by treatment with p38 and ROS inhibitors (Fig. 9g). These results indicate that the ROS production that resulted from PP stimulation contributed to NF-κB activation via p38 phosphorylation (Fig. 10).

3. Discussion

The molecular mechanisms of toxicity responses such as inflammation and ROS production to PP stimulation were investigated both *in vivo* and *in vitro*. Our results showed increased inflammatory cells, cytokines, and chemokines in the BALF of PP-instilled mice, alongside higher ROS production in the lung tissues, as compared to the VC group. Histopathological analysis of the lung tissue of PP-instilled mice revealed lung damage, including the infiltration of inflammatory cells in the perivascular/parenchymal space, alveolar epithelial hyperplasia, and foamy macrophage aggregates. *In vitro* investigation revealed depolarisation of the mitochondrial membrane potential, decreased ATP levels, and ROS production as a result of PP stimulation. PP was also found to induce the production of inflammatory cytokines (TNF-α, IL-1β, and IL-6) and cell death, with an increase in the levels of p-p38 and p-NF-κB protein observed both *in vivo* and *in vitro*. Interestingly, p38 and ROS inhibition regulated toxic responses such as inflammatory cytokines and cell death. These results suggest that PP stimulation might contribute to the pathogenesis of inflammation within the respiratory system via NF-κB signaling, which is associated with mitochondrial damage (Fig. 10).

With advancements in technology, the exposure to airborne microparticles such as PM in daily life has been increasing. Microparticles can form as a result of industrial processes, with other sources including traffic or road construction [23, 28–30]. Recent studies have reported that various plastics, including PP, PS, and PET were detected in the atmosphere in various forms (particles, fibres, and vinyl) [3–6]. Recent studies have reported that submillimetre microplastic fragments (PP, PET, PS, and polyvinyl chloride) have been detected in human lung tissue, with PP microplastics the most frequently observed (both in particulate and fibrous form) [11]. Interestingly, other studies have reported the detection of 12 different microplastic polymers in the lung tissue of live humans, with PP (23%), PET (18%), resin (15%), and PE (10%) the most abundant [10]. This exposure to persistent matter, including microplastics, can lead to respiratory diseases, and chronic exposure to persistent matter has been reported to cause cancer after 10 to 20 years [12, 31–34]. Several studies have reported the risks of inhalation exposure to humans, however, the toxicity mechanisms of microplastics in the respiratory system remain poorly understood.

Recent various studies have evaluated toxicologic effects of microplastic, hypothesizing that microplastic in the atmosphere might cause risk to the respiratory system by inhalation exposure in humans. Microplastics are known to induce lung inflammation by lung infiltration through the upper and lower airways as a result of inhalation exposure. Moreover, the inhalation of nanosized plastic can lead to bronchial epithelial injury by epithelial barrier infiltration [3, 12]. Recent studies investigating the effects of microplastics on lung epithelial cells have reported that PS microplastic exposure induces inflammatory cytokines and cytotoxicity owing to the cellular uptake of particles in A549 cells [26]. In other studies, the exposure of A549 cells to PS nano-plastics over 24 h led to the accumulation of the particles, which led to the production of inflammatory cytokines and oxidative stress, with ROS production and lipid peroxidation observed [35]. As mentioned above, PS has been investigated in several toxicology and physiology studies, as it finds usage in various products owing to its remarkable thermoplastic polymer properties [36]. However, investigations on the toxicity of PP, the primary material in disposable products, are scarce. With the increased usage of disposable products, PP microplastic has aroused concerns about possibile adverse effects in humans. Interestngly, recent studies have reported that PP was

detected in body organs including the lung of humans [10, 11]. For this reason, toxicity studies on PP are necessary. Our results showed that ROS production, inflammatory cytokines, and cytotoxicity were significantly increased in PP-exposed A549 cells as compared to the control (Fig. 7), and alveolar epithelial hyperplasia and inflammatory cell infiltration were observed in the histopathological results of PP-instilled mice (Fig. 3). These results suggest that PP microplastics stimulation might contribute to the pulmonary toxic response through lung epithelium injury.

Our results showed that the number of inflammatory cells, including macrophages, neutrophils, and lymphocytes in the BALF of PP-instilled mice increased in a dose-dependent manner as compared to the VC. Neutrophils, which are the most common leukocytes and are essential first responders during the initial phases of inflammation, were predominant in the BALF of PP-instilled mice (Fig. 2a). The granulation and activation of neutrophils causes pulmonary inflammation via the release of various inflammatory cytokines and chemokines [37–39]. Especially, helper T (Th) cytokines play important roles in inflammatory responses in pulmonary diseases such as asthma and pulmonary fibrosis [40, 41]. Previous studies reported that IL-17 overexpression and neutrophil accumulation in BALF of mice with diesel exhaust particulates (DEP)-induced lung inflammation were observed and that the Th17 pathway might be involved in DEP-induced inflammation [23]. We investigated the gene expression patterns after PP exposure to reveal the molecular mechanism associated with PP-induced lung inflammation. We observed that the expressions of Th17 signaling pathway-associated genes including those encoding C-C motif chemokine ligand (CCL) 2, CCL12, CCL17, CXCL1, and CXCL5 were increased in the lung tissue of PP-instilled mice. We presume that, PP stimulation might have induced lung inflammation through the Th17 signaling pathway (data not shown). Recently, nanoparticles such as TiO2, CeO2, and ZnO have been reported to activate neutrophil degranulation, inducing inflammatory tissue injury [42–44]. PM-instilled mice have previously been shown to suffer from an increase in the number of neutrophils followed by the release of inflammatory cytokines and chemokines [45]. Interestingly, our results showed that inflammatory cytokines and chemokines such as TNF-α, IL-1β, IL-6, MCP-1, and CXCL1/KC in the BALF of PP-instilled mice increased in a dose-dependent manner, and the histopathological results of PP-instilled mice showed inflammatory cell infiltration (Fig. 2b-f, Fig. 3). These results indicate that PP microparticle stimulation may contribute to neutrophilic lung inflammation.

Oxidative stress and endoplasmic reticulum (ER) stress resulting from cellular organelle injury caused by exposure to environmental factors such as chemicals and pathogens can lead to various diseases including pulmonary diseases via abnormal inflammation and immune responses [19, 20, 46, 47]. Our results show that PP-exposed A549 cells had significantly increased ROS production and levels of antioxidant enzymes including catalase (CAT), superoxide dismutase (SOD)1, SOD2, and glutathione peroxidase-1 (GPX1). However, the protein levels of ER stress markers such as binding immunoglobulin protein (BiP) and C/EBP homologous protein (CHOP) were unchanged (Supplementary 1, 2). Interestingly, nuclear factor erythroid-2-related factor 2 (Nrf2) protein levels (total and nuclear) in PP-exposed A549 cells were significantly increased compared to the control, which might have regulated the expression of antioxidant proteins that protect against oxidative damage (Supplementary 3). Despite the need for more studies, we speculate that oxidative stress may be an indirect result of mitochondrial damage. Previous

studies have reported that nanoparticles can damage mitochondria, and induce toxicity [27, 48–50]. Recent studies have reported that ultrafine dust exposure induced oxidative stress and mitochondrial damage in bronchial epithelial cells (BEAS-2B) and monocyte/macrophage cell lines (RAW 264.7 cells) [27]. NH_2-PS stimulation induces mitochondrial dysfunction, leading to decreased ATP levels, DNA degradation, and a decline in the mitochondrial membrane potential of BEAS-2B and RAW 264.7 cells [48]. Our results showed that PP exposure induces mitochondrial dysfunctions such as mitochondrial depolarization and decreases ATP levels (Fig. 5). Interestingly, DRP1 proteins merged into the damaged mitochondrial regions (Fig. 6), which might be a quality control mechanism for preserving a healthy mitochondrial network via fission [51]. These results suggest that PP stimulation causes mitochondrial damage and that long-term PP microplastic exposure may potentially lead to mitochondrial diseases.

Recent studies have reported that airborne microplastics cause inflammation through various pathogenesis, such as dust overload, oxidative stress, and cytotoxicity [52–55]. In particular, ROS overproduction by particle exposure-induced inflammation and cytotoxicity is mediated by the release of cytokines and inflammatory mediators due to the translocation of nuclear factor NF-κB in cell signaling pathways [56–58]. Various studies have reported that oxidative stress causes NF-κB activation via the phosphorylation of MAPKs such as p38, ERK, and JNK, which regulate important cellular processes such as proliferation, stress responses, apoptosis, and immune defense [24, 25, 59–61]. Recent studies have reported that the persistent activation of p38 significantly contributes to the pathogenesis of Th2 low neutrophilic inflammation, which is associated with severe asthmatic phenotypes [62]. In addition, cigarette smoke-treated mice have shown p38 activation and release of pro-inflammatory cytokines and chemokines, which lead to neutrophilic lung inflammation. These findings are in agreement with the results obtained from chronic obstructive pulmonary disease (COPD) patients [63, 64]. In asthmatic patients, activated p38 MAPK contributed to TNF-α secretion from natural killer (NK) cells stimulated by IL-12, and the secretion of IL-6, IL-8, and MCP-1 were also partially dependent upon p38 activation [65, 66]. Interestingly, recent studies have reported that apoptosis was induced through p38 signaling by hydrogen peroxide, which is used as an oxidative stress inducer [67]. We demonstrated that PP stimulation caused inflammatory response, oxidative stress, and cell death. Interestingly, we also observed that the inflammatory cytokines and cell death induced by PP stimulation were reduced by p38 and ROS inhibitors (Fig. 9). These results suggest that lung neutrophilic inflammation via PP stimulation may be a potential therapeutic target that includes p38 inhibition.

4. Conclusions

The toxicological effects that PP microplastics have on the respiratory system were investigated, with results indicating that PP stimulation leads to lung inflammation *in vivo*. PP exposure causes mitochondrial injury and cytotoxicity manifested as ROS production, inflammatory responses, and cell death *in vitro*. Inflammation and cell death of PP-exposed A549 cells were reversed by p38 and ROS inhibition. These results suggest that PP microplastics contribute to the pathogenesis of inflammation via p38-mediated NF-κB signaling, resulting from mitochondrial injury in the respiratory systems.

5. Methods

5.1 PP nanoplastics

PP particles were prepared by precipitating a solution dissolved at 200°C on a hot plate with PP beads (Sigma, 428116) and xylene (DAEJUNG, 8587 – 4410) solvent with ethanol. Field emission scanning electron microscopy (FE-SEM; JSM-7100F) analysis was performed to measure the size of the PP particles, and dynamic light scattering (DLS; ELSZ-2000) was used to measure the sizes of the PP particles with regards to their dispersal in the liquid. Dispersion stability was measured using Turbiscan (Turbiscan LAB) in both *in vivo* and *in vitro* experiments.

5.2 Animals and experimental design

Seven-week-old male ICR mice were purchased from Orient Bio Inc. (Seongnam, Korea). The mice were housed in a temperature-controlled environment (22 ± 3°C) with a relative humidity of 50 ± 20%, a 12 h light/dark cycle, and ventilated with air (10–20 times/h). The mice were provided with pellets that are specifically produced for experimental animals (PMI Nutrition International, Richmond, IN, USA) and UV-irradiated (Steritron SX-1; Daeyoung, Seoul, Korea) and filtered (1 μm-pore filter) tap water. All experimental procedures were approved by the Institutional Animal Care and Use Committee at the Korea Institute of Toxicology (IACUC #2108-0003). The mice in the PP groups received intratracheal instillation of 1, 2.5, or 5 mg/kg PP in 50 μl saline solution five times per week for 4 weeks using an automatic video instillator [68]. The mice in the VC group were instilled with saline using the same method. The mice were sacrificed on day 29.

5.3 Cell culture and treatment

A549 cells were obtained from the American Type Culture Collection (ATCC). Cells were grown in RPMI 1640 medium (Gibco) containing 10% inactivated fetal bovine serum (FBS; Gibco). The A549 cells were incubated at 37°C in a humidified 5% CO2 atmosphere and treated with PP (1, 2, and 4 mg/ml) overnight. The mitochondrial ROS inhibitor N-acetyl-L-cysteine (NAC; Sigma, A7250) was added 6 h before PP treatment. A p38 MAP kinase inhibitor (Sigma, SML0543) was added 2 h before PP treatment.

5.4 BALF preparation

At 24 h after the last PP intratracheal instillation, the mice were anesthetized with isoflurane and exsanguinated. The left lung was ligated, and the right lung was gently lavaged three times via the tracheal tube with a total volume of 0.7 mL phosphate-buffered saline (PBS; Gibco). The collected solutions were pooled and maintained at 4 °C. BAL cells were prepared using Cytospin (Thermo Fisher Scientific) and stained with Diff-Quik solution (Dade Diagnostics, Aguada, Puerto, USA). A total of 200 cells were counted at each slide.

5.5 Measurement of inflammatory cytokine and chemokine levels in BALF

The TNF-α, IL-1β, IL-6, MCP-1, and KC levels in BALF were quantified by ELISA using a commercial kit (R&D Systems) in accordance with the manufacturer's protocols.

5.6 Histopathological analysis

The left lung of each mice was fixed with 10% neutral-buffered formalin (NRF). The specimens were dehydrated and embedded in paraffin to produce tissue blocks which were sectioned into 4-μm thick slices. Lung sections from each animal were stained with haematoxylin and eosin (H&E). All samples were analysed using a Leica DM2500 microscope (Leica Instruments, Wetzlar, Germany) at 200 × and 400 × magnifications. The degree of lung injury in each animal was scored on a scale ranging from 0 to 4.

5.7 Cell viability and ROS measurement

Cell viability was evaluated using an MTT assay (Sigma, M2128). To determine cell viability, a 1 mg/ml MTT solution was added to the cells after PP stimulation before incubation at 37°C for 3 h. Absorbance was measured using Synergy Mx microplate reader (BioTek) at OD 570 nm. ROS levels in the lung tissue of PP-instilled mice were quantified using commercial ELISA kits (Abbkine, KTE71621) in accordance with the manufacturer's protocols. The cells were then incubated with 3% serum in PBS containing 1 μM CM-H2DCFDA dye for 30 min at 37°C and the number of stained cells determined using a flow cytometer (Beckman Coulter). Mitochondrial ROS levels were measured using MitoTracker Red CM-H2XRos (Invitrogen, M7513) and MitoTracker Green FM (Invitrogen, M7514). Staining was incubated with 3% serum in PBS containing 200 nM of Mitotracker Red CM-H2XRos and MitoTracker Green FM for 30 min at 37°C. Stained cells were analysed using a Zeiss lsm 800 confocal microscope (Carl Zeiss) at 400 × magnification.

5.8 Preparation of cell lysates and western blot analysis

Cell lysates were homogenised in the presence of a protease inhibitor cocktail with RIPA buffer (Thermo Fisher Scientific). Nuclear extracts were homogenised using a nuclear and cytoplasmic extraction kit (Thermo Fisher Scientific, 78835) according to the instructions of the manufacturer. Protein concentrations were determined using Bradford reagent (Bio-Rad). The samples were then loaded onto an SDS-PAGE gel. After electrophoresis at 90 V for 120 min, the protein was transferred to polyvinylidene difluoride membranes (Merck Millipore) at 250 mA over 60 min using a transfer method. Nonspecific sites were blocked with 5% non-fat dry milk in Tris-buffered saline/Tween 20 (TBS-T) for 1 h and incubated with DRP1 (NOVUS, NB110-55288), MFN1 (Proteintech, 13798-1-AP), MFN2 (Proteintech, 12186-1-AP), Lamin B (Cell signaling, 9087S), p-p38 (Cell signaling, 4511S), p38 (Cell signaling, 8690S), p-ERK (Cell signaling, 4370S), ERK (Cell signaling, 4695S), p-JNK (Cell signaling, 4668T), JNK (Cell signaling, 9252S), p-IκB-α (Cell signaling, 9246S), IκB-α (Cell signaling, 4812S), p-NF-κB (Cell signaling, 3033S), NF-κB (Cell signaling, 8242S), IL-1β (Abcam, ab9722), IL-6 (Invitrogen, P620), TNF-α (Abcam, ab66579), CAT (Abcam, ab16731), SOD1 (Abcam, ab16831), SOD2 (R&D Systems, MAB3419), GPX1 (Abcam, ab108427), BiP (Cell signaling, 3183S), CHOP (Cell signaling, 2895S), Nrf2 (Cell signaling, 12721S), and β-actin (Santa Cruz, sc-47778) overnight at 4 ℃. Anti-rabbit (Cell signaling, 7074S) and anti-mouse (Cell signaling,

7076S) horseradish peroxidase-conjugated IgG was used to detect antibody binding. The binding of specific antibodies was visualized using the iBright CL 1000 imaging system (Thermo Fisher Scientific) after treatment with the ECL reagent (Thermo Fisher Scientific). The results of the densitometric analysis were expressed as the relative ratio of the target protein to the reference protein. The relative ratio of the target protein to the control was arbitrarily denoted 1.

5.9 Measurement of mitochondrial membrane potential

Mitochondrial membrane potential was measured using JC-1 dye (Invitrogen, T3168). Cells were incubated with 3% serum in PBS containing 2.5 μg/ml of JC-1 for 30 min at 37°C. Stained cells were analysed using a Zeiss lsm 800 confocal microscopes (Carl Zeiss) at 400 × magnification. The cells were scanned by dual excitation with 488 nm (green) and 568 nm (red) laser lines.

5.10 Immunofluorescence staining and confocal microscopy

Cells were fixed in methanol at − 20°C for 3 min. After washing with PBS, the cells were blocked with 1% BSA in PBS-T for 30 min. Cells were then washed three times with PBS and incubated overnight at 4°C with TOM20 (Santa Cruz, sc-17764) and DRP1 (NOVUS, NB110-55288). The sections were treated with Alexa Fluor 488 anti-mouse (Invitrogen, A11001) and Alexa Fluor 594 anti-rabbit (Invitrogen, A11037) for 2 h at RT. Stained cells were analysed using a Zeiss lsm 800 confocal microscopes (Carl Zeiss) at 400 × magnification.

5.11 Analysis of ATP levels

ATP levels were assessed using a colorimetric ATP assay kit (Abcam, ab83355), according to the instructions of the manufacturer. ATP levels were measured using a Synergy Mx microplate reader (BioTek) at 570 nm.

5.12 Statistical analysis

Statistical analysis was performed using GraphPad InStat v. 3.0 (GraphPad Software, Inc., La Jolla, CA, USA). Statistical comparisons were performed using one-way ANOVA followed by Dunnett's multiple comparison test, and statistical comparisons between two groups were performed using the Student's t-test. Data are presented as the mean ± SD. A value of $p < 0.05$ was considered statistically significant.

Abbreviations

ATP: Adenosine triphosphate; BiP: Binding immunoglobulin protein; BALF: Bronchoalveolar lavage fluid; CAT: Catalase; CCL: C-C motif chemokine ligand; CHOP: C/EBP homologous protein; COPD: Chronic obstructive pulmonary disease; CXCL1/KC: C-X-C motif chemokine ligand 1; DEP: Diesel exhaust particulates; DRP1: Dynamin-related protein 1; ER: Endoplasmic reticulum; ERK: Extracellular signal-regulated kinases; GPX1: Glutathione peroxidase-1; JNK: C-Jun N-terminal kinases; IL: Interleukin; MFN1:

Mitofusin 1; MFN2: Mitofusin 2; MAPK: Mitogen-activated protein kinase; MCP-1: Monocyte chemoattractant protein-1; NK: Natural killer; Nrf2: Nuclear factor erythroid-2-related factor 2; NF-κB: nuclear factor kappa B; PM: Particulate matter; PE: Polyethylene; PET: Polyethylene terephthalate; PP: Polypropylene; PS: Polystyrene; ROS: Reactive oxygen species; SOD: Superoxide dismutase; Th: Helper T; TNF-α: Tumor necrosis factor-α; VC: Vehicle control.

Declarations

Acknowledgements

Not applicable.

Authors' contributions

JHW: Methodology, Conceptualization, Formal analysis, Investigation, Writing—original draft, Writing—review and editing. SHJ: Methodology, Formal analysis, Investigation, Writing—review and editing. LJY: Methodology, Conceptualization, Investigation, Writing—review and editing. LI: Methodology, Conceptualization, Investigation, Writing—review and editing. JK: Methodology, Conceptualization, Investigation, Writing—review and editing. KB: Formal analysis, Writing—review and editing, Supervision. LK: Conceptualization, Writing—review and editing, Supervision, Funding acquisition, Project administration. All authors read and approved the final manuscript.

Funding

This work was supported by the Korea Environmental Industry & Technology Institute (Grant No. HE-2203).

Availability of data and materials

The datasets used and/or analyzed during the current study are available from the corresponding author on reasonable request.

Ethics approval and consent to participate

All animal management was in accordance with the ethical rules of the Institutional Animal Care and Use Committee of the Korea Institute of Toxicology (Number: 2108-0003).

Consent for publication

All authors have consented for publication.

Competing interests

The authors declare that they have no competing interests.

Authors details

[1]Inhalation Toxicology Center for Airborne Risk Factor, Korea Institute of Toxicology, 30 Baehak1-gil, Jeongeup, Jeollabuk-do, 56212, Republic of Korea. [2]Biosafety Research Institute and Laboratory of Pathology, College of Veterinary Medicine, Jeonbuk National University, Iksan-si, Jeollabuk do, Republic of Korea. [3]Department of Human and Environmental Toxicology, University of Science & Technology, Daejeon, 34113, Republic of Korea. [4]Korea Radioisotope Center for Pharmaceuticals, Korea Radiological and Medical Sciences, 75 Nowon-ro, Nowon-gu, Seoul, 01812, Republic of Korea. [5] VITALS Co., Ltd., 30 Gukjegwahak 3-ro, Yuseong-hu, Daejeon, 34000, Republic of Korea.

References

1. Andrady AL, Neal MA. Applications and societal benefits of plastics. Philos Trans R Soc Lond B Biol Sci. 2009;364:1977–84. https://doi.org/10.1098/rstb.2008.0304
2. Jung S, Yang JY, Byeon EY, Kim DG, Lee DG, Ryoo S, et al. Copper-Coated Polypropylene Filter Face Mask with SARS-CoV-2 Antiviral Ability. Polymers (Basel). 2021;13:1367. https://doi.org/10.3390/polym13091367
3. Wright SL, Kelly FJ. Plastic and Human Health: A Micro Issue? Environ Sci Technol. 2017;51:6634–6647. https://doi.org/10.1021/acs.est.7b00423
4. Prata JC. Airborne microplastics: consequences to human health? Environ Pollut. 2018;234:115–126. https://doi.org/10.1016/j.envpol.2017.11.043
5. Brahney J, Mahowald N, Prank M, Cornwell G, Klimont Z, Matsui H, et al. Constraining the atmospheric limb of the plastic cycle. Proc Natl Acad Sci U S A. 2021;118:e2020719118. https://doi.org/10.1073/pnas.2020719118
6. Brahney J, Hallerud M, Heim E, Hahnenberger M, Sukumaran S. Plastic rain in protected areas of the United States. Science. 2020;368:1257–1260. https://doi.org/10.1126/science.aaz5819
7. Brussow H, Zuber S. Can a combination of vaccination and face mask wearing contain the COVID-19 pandemic? Microb Biotechnol. 2022;15:721–737. https://doi.org/10.1111/1751-7915.13997
8. Roberts KP, Phang SC, Williams JB, Hutchinson DJ, Kolstoe SE, Bie J, et al. Increased personal protective equipment litter as a result of COVID-19 measures. Nature Sustainability. 2022;5:272–279. https://doi.org/10.1038/s41893-021-00824-1
9. Atis S, Tutluoglu B, Levent E, Ozturk C, Tunaci A, Sahin K, et al. The respiratory effects of occupational polypropylene flock exposure. Eur Respir J. 2005;25:110–7. https://doi.org/10.1183/09031936.04.00138403
10. Jenner LC, Rotchell JM, Bennett R, Cowen M, Tentzeris V, Sadofsky LR. Detection of microplastics in human lung tissue using μFTIR spectroscopy. Sci Total Environ. 2022;831:154907. https://doi.org/10.1016/j.scitotenv.2022.154907

11. Amato-Lourenco LF, Carvalho-Oliveira R, Junior GR, Galvao LDS, Ando RA, Mauad T. Presence of airborne microplastics in human lung tissue. J Hazard Mater. 2021;416:126124. https://doi.org/10.1016/j.jhazmat.2021.126124
12. Facciola A, Visalli G, Ciarello MP, Pietro AD. Newly Emerging Airborne Pollutants: Current Knowledge of Health Impact of Micro and Nanoplastics. Int J Environ Res Public Health. 2021;18:2997. https://doi.org/10.3390/ijerph18062997
13. Elsaesser A, Howard CV. Toxicology of nanoparticles. Adv Drug Deliv Rev. 2012;64:129–37. https://doi.org/10.1016/j.addr.2011.09.001
14. Kannan K, Vimalkumar K. A Review of Human Exposure to Microplastics and Insights Into Microplastics as Obesogens. Front Endocrinol (Lausanne). 2021;12:724989. https://doi.org/10.3389/fendo.2021.724989
15. Bratic I, Trifunovic A. Mitochondrial energy metabolism and ageing. Biochim Biophys Acta. 2010;1797:961–7. https://doi.org/10.1016/j.bbabio.2010.01.004
16. Wiemerslage L, Lee D. Quantification of Mitochondrial Morphology in Neurites of Dopaminergic Neurons using Multiple Parameters. J Neurosci Methods. 2016;262:56–65. https://doi.org/10.1016/j.jneumeth.2016.01.008
17. Kim SR, Kim DI, Kim SH, Lee H, Lee KS, Cho SH, et al. NLRP3 inflammasome activation by mitochondrial ROS in bronchial epithelial cells is required for allergic inflammation. Cell Death Dis. 2014;5:e1498. https://doi.org/10.1038/cddis.2014.460
18. Rangarajan S, Bernard K, Thannickal VJ. Mitochondrial Dysfunction in Pulmonary Fibrosis. Ann Am Thorac Soc. 2017;14:S383-S388. https://doi.org/10.1513/annalsats.201705-370aw
19. Lim YA, Rhein V, Baysang G, Meier F, Poljak A, Raftery MJ, et al. Abeta and human amylin share a common toxicity pathway via mitochondrial dysfunction. Proteomics. 2010;10:1621–33. https://doi.org/10.1002/pmic.200900651
20. Shukla A, Timblin C, Berube K, Gordon T, Mckinney W, Driscoll K, et al. Inhaled particulate matter causes expression of nuclear factor (NF)-kappaB-related genes and oxidant-dependent NF-kappaB activation in vitro. Am J Respir Cell Mol Biol. 2000;23:182–7. https://doi.org/10.1165/ajrcmb.23.2.4035
21. Wang J, Huang J, Wang L, Chen C, Yang D, Jin M, et al. Urban particulate matter triggers lung inflammation via the ROS-MAPK-NF-κB signaling pathway. J Thorac Dis. 2017;9:4398–4412. https://doi.org/10.21037/jtd.2017.09.135
22. Visalli G, Facciola A, Curro M, Lagana P, Fauci VL, Iannazzo D, et al. Mitochondrial Impairment Induced by Sub-Chronic Exposure to Multi-Walled Carbon Nanotubes. Int J Environ Res Public Health. 2019;16:792. https://doi.org/10.3390/ijerph16050792
23. Kim DI, Song MK, Kim HI, Han KM, Lee K. Diesel Exhaust Particulates Induce Neutrophilic Lung Inflammation by Modulating Endoplasmic Reticulum Stress-Mediated CXCL1/KC Expression in Alveolar Macrophages. Molecules. 2020;25:6046. https://doi.org/10.3390/molecules25246046

24. Saha RN, Jana M, Pahan K. MAPK p38 regulates transcriptional activity of NF-kappaB in primary human astrocytes via acetylation of p65. J Immunol. 2007;179:7101–9. https://doi.org/10.4049/jimmunol.179.10.7101
25. Schulze-Osthoff K, Ferrari D, Riehemann K, Wesselborg S. Regulation of NF-kappa B activation by MAP kinase cascades. Immunobiology. 1997;198:35–49. https://doi.org/10.1016/s0171-2985(97)80025-3
26. Xu M, Halimu G, Zhang Q, Song Y, Fu X, Li Y, et al. Internalization and toxicity: A preliminary study of effects of nanoplastic particles on human lung epithelial cell. Sci Total Environ. 2019;694:133794. https://doi.org/10.1016/j.scitotenv.2019.133794
27. Li N, Sioutas C, Cho A, Schmitz D, Misra C, Sempf J, et al. Ultrafine particulate pollutants induce oxidative stress and mitochondrial damage. Environ Health Perspect. 2003;111:455–60. https://doi.org/10.1289/ehp.6000
28. Kurt OK, Zhang J, Pinkerton KE. Pulmonary health effects of air pollution. Curr Opin Pulm Med. 2016;22:138–43. https://doi.org/10.1097/mcp.0000000000000248
29. Falcon-Rodriguez CI, Osornio-Vargas AR, Sada-Ovalle I, Segura-Medina P. Aeroparticles, Composition, and Lung Diseases. Front Immunol. 2016;7:3. https://doi.org/10.3389/fimmu.2016.00003
30. Jia YY, Wang Q, Liu T. Toxicity Research of PM 2.5 Compositions In Vitro. Int J Environ Res Public Health. 2017;14:232. https://doi.org/10.3390/ijerph14030232
31. Goldberg MS, Theriault G. Retrospective cohort study of workers of a synthetic textiles plant in Quebec: II. Colorectal cancer mortality and incidence. Am J Ind Med. 1994;25:909–22. https://doi.org/10.1002/ajim.4700250613
32. Zuskin E, Mustajbegovic J, Schachter EN, Kern J, Budak A, Godnic-Cvar J. Respiratory findings in synthetic textile workers. Am J Ind Med. 1998;33:263–73. https://doi.org/10.1002/(sici)1097-0274(199803)33:3%3C263::aid-ajim8%3E3.0.co;2-x
33. Acquavella JF, Douglass TS, Phillips SC. Evaluation of excess colorectal cancer incidence among workers involved in the manufacture of polypropylene. J Occup Med. 1988;30:438–42. https://doi.org/10.1097/00043764-198805000-00012
34. Mastrangelo G, Fedeli U, Fadda E, Milan G, Lange JH. Epidemiologic evidence of cancer risk in textile industry workers: a review and update. Toxicol Ind Health. 2002;18:171–81. https://doi.org/10.1191/0748233702th139rr
35. Shi Q, Tang J, Wang L, Liu R, Giesy JP. Combined cytotoxicity of polystyrene nanoplastics and phthalate esters on human lung epithelial A549 cells and its mechanism. Ecotoxicol Environ Saf. 2021;213:112041. https://doi.org/10.1016/j.ecoenv.2021.112041
36. Bonanomi M, Salmistraro N, Porro D, Pinsino A, Colangelo AM, Gaglio D. Polystyrene micro and nano-particles induce metabolic rewiring in normal human colon cells: A risk factor for human health. Chemosphere. 2022;303:134947. https://doi.org/10.1016/j.chemosphere.2022.134947
37. Tomonaga T, Izumi H, Oyabu T, Lee BW, Kubo M, Shimada M, et al. Assessment of Cytokine-Induced Neutrophil Chemoattractants as Biomarkers for Prediction of Pulmonary Toxicity of Nanomaterials.

Nanomaterials (Basel). 2020;10:1563. https://doi.org/10.3390/nano10081563

38. Morimoto Y, Izumi H, Kuroda E. Significance of persistent inflammation in respiratory disorders induced by nanoparticles. J Immunol Res. 2014;2014:962871. https://doi.org/10.1155/2014/962871
39. Borm PJ, Driscoll K. Particles, inflammation and respiratory tract carcinogenesis. Toxicol Lett. 1996;88:109–13. https://doi.org/10.1016/0378-4274(96)03725-3
40. Chapman DG, Tully JE, Nolin JD, Janssen-Heininger YM, Irvin CG. Animal models of allergic airways disease: where are we and where to next? J Cell Biochem. 2014;115:2055–64. https://doi.org/10.1002/jcb.24881
41. Erle DJ, Sheppard D. The cell biology of asthma. J Cell Biol. 2014;205:621–31. https://doi.org/10.1083/jcb.201401050
42. Garcia G, Kim MH, Morikis VA, Simon SI. Neutrophil Inflammatory Response Is Downregulated by Uptake of Superparamagnetic Iron Oxide Nanoparticle Therapeutics. Front Immunol. 2020;11:571489. https://doi.org/10.3389/fimmu.2020.571489
43. Babin K, Antoine F, Goncalves DM, Girard D. TiO2, CeO2 and ZnO nanoparticles and modulation of the degranulation process in human neutrophils. Toxicol Lett. 2013;221:57–63. https://doi.org/10.1016/j.toxlet.2013.05.010
44. Couto D, Freitas M, Vilas-Boas V, Dias I, Proto G, Lopez-Quintela MA, et al. Interaction of polyacrylic acid coated and non-coated iron oxide nanoparticles with human neutrophils. Toxicol Lett. 2014;225:57–65. https://doi.org/10.1016/j.toxlet.2013.11.020
45. He M, Ichinose T, Yoshida Y, Arashidani K, Yoshida S, Takano H, et al. Urban PM2.5 exacerbates allergic inflammation in the murine lung via a TLR2/TLR4/MyD88-signaling pathway. Sci Rep. 2017;7:11027. https://doi.org/10.1038/s41598-017-11471-y
46. Kim SJ, Cheresh P, Jablonski RP, Williams DB, Kamp DW. The Role of Mitochondrial DNA in Mediating Alveolar Epithelial Cell Apoptosis and Pulmonary Fibrosis. Int J Mol Sci. 2015;16:21486–21519. https://doi.org/10.3390/ijms160921486
47. Jeong JS, Kim SR, Cho SH, Lee YC. Endoplasmic Reticulum Stress and Allergic Diseases. Curr Allergy Asthma Rep. 2017;17:82. https://doi.org/10.1007/s11882-017-0751-9
48. Xia T, Kovochich M, Liong M, Zink JI, Nel AE. Cationic polystyrene nanosphere toxicity depends on cell-specific endocytic and mitochondrial injury pathways. ACS Nano. 2008;2:85–96. https://doi.org/10.1021/nn700256c
49. Stern ST, Adiseshaiah PP, Crist RM. Autophagy and lysosomal dysfunction as emerging mechanisms of nanomaterial toxicity. Part Fibre Toxicol. 2012;9:20. https://doi.org/10.1186/1743-8977-9-20
50. Xia T, Korge P, Weiss JN, Li N, Venkatesen MI, Sioutas C, et al. Quinones and aromatic chemical compounds in particulate matter induce mitochondrial dysfunction: implications for ultrafine particle toxicity. Environ Health Perspect. 2004;112:1347–58. https://doi.org/10.1289/ehp.7167
51. Tilokani L, Nagashima S, Paupe V, Prudent J. Mitochondrial dynamics: overview of molecular mechanisms. Essays Biochem. 2018;62:341–360. https://doi.org/10.1042/ebc20170104

52. Hoelting L, Scheinhardt B, Bondarenko O, Schildknecht S, Kapitza M, Tanavde V, et al. A 3-dimensional human embryonic stem cell (hESC)-derived model to detect developmental neurotoxicity of nanoparticles. Arch Toxicol. 2013;87:721–33. https://doi.org/10.1007/s00204-012-0984-2
53. Murali K, Kenesei K, Li Y, Demeter K, Kornyei Z, Madarasz E. Uptake and bio-reactivity of polystyrene nanoparticles is affected by surface modifications, ageing and LPS adsorption: in vitro studies on neural tissue cells. Nanoscale. 2015;7:4199–210. https://doi.org/10.1039/c4nr06849a
54. Schirinzi GF, Perez-Pomeda I, Sanchis J, Rossini C, Farre M, Barcelo D. Cytotoxic effects of commonly used nanomaterials and microplastics on cerebral and epithelial human cells. Environ Res. 2017;159:579–587. https://doi.org/10.1016/j.envres.2017.08.043
55. Poma A, Vecchiotti G, Colafarina S, Zarivi O, Aloisi M, Arrizza L, et al. In Vitro Genotoxicity of Polystyrene Nanoparticles on the Human Fibroblast Hs27 Cell Line. Nanomaterials (Basel). 2019;9:1299. https://doi.org/10.3390/nano9091299
56. Donaldson K, Tran CL. Inflammation caused by particles and fibers. Inhal Toxicol. 2002;14:5–27. https://doi.org/10.1080/089583701753338613
57. Chang C. The immune effects of naturally occurring and synthetic nanoparticles. J Autoimmun. 2010;34:J234-46. https://doi.org/10.1016/j.jaut.2009.11.009
58. Xia T, Kovochich M, Brant J, Hotze M, Sempf J, Oberley T, et al. Comparison of the abilities of ambient and manufactured nanoparticles to induce cellular toxicity according to an oxidative stress paradigm. Nano Lett. 2006;6:1794–807. https://doi.org/10.1021/nl061025k
59. Soares-Silva M, Diniz FF, Gomes GN, Bahia D. The Mitogen-Activated Protein Kinase (MAPK) Pathway: Role in Immune Evasion by Trypanosomatids. Front Microbiol. 2016;7:183. https://doi.org/10.3389/fmicb.2016.00183
60. Son Y, Cheong YK, Kim NH, Chung HT, Kang DG, Pae HO. Mitogen-Activated Protein Kinases and Reactive Oxygen Species: How Can ROS Activate MAPK Pathways? J Signal Transduct. 2011;2011:792639. https://doi.org/10.1155/2011/792639
61. Mccubrey JA, Lahair MM, Franklin RA. Reactive oxygen species-induced activation of the MAP kinase signaling pathways. Antioxid Redox Signal. 2006;8:1775–89. https://doi.org/10.1089/ars.2006.8.1775
62. Ray A, Kolls JK. Neutrophilic Inflammation in Asthma and Association with Disease Severity. Trends Immunol. 2017;38:942–954. https://doi.org/10.1016/j.it.2017.07.003
63. Marumo S, Hoshino Y, Kiyokawa H, Tanabe N, Sato A, Ogawa E, et al. p38 mitogen-activated protein kinase determines the susceptibility to cigarette smoke-induced emphysema in mice. BMC Pulm Med. 20147;14:79. https://doi.org/10.1186/1471-2466-14-79
64. Wang C, Zhou J, Wang J, Li S, Fukunaga A, Yodoi J, et al. Progress in the mechanism and targeted drug therapy for COPD. Signal Transduct Target Ther. 2020;5:248. https://doi.org/10.1038/s41392-020-00345-x
65. Ochayon DE, Ali A, Alarcon PC, Krishnamurthy D, Kottyan LC, Borchers MT, et al. IL-33 promotes type 1 cytokine expression via p38 MAPK in human NK cells. J Leukoc Biol. 2020;107:663–671.

https://doi.org/10.1002/jlb.3a0120-379rr

66. Kim DH, Gu A, Lee JS, Yang EJ, Kashif A, Hong MH, et al. Suppressive effects of S100A8 and S100A9 on neutrophil apoptosis by cytokine release of human bronchial epithelial cells in asthma. Int J Med Sci. 2020;17:498–509. https://doi.org/10.7150/ijms.37833
67. Barata AG, Dick TP. A role for peroxiredoxins in H_2O_2- and MEKK-dependent activation of the p38 signaling pathway. Redox Biol. 2020;28:101340. https://doi.org/10.1016/j.redox.2019.101340
68. Kim JS, Lee B, Hwang IC, Yang YS, Yang MJ, Song CW. An automatic video instillator for intratracheal instillation in the rat. Lab Anim. 2010;44:20–4. https://doi.org/10.1258/la.2009.009003

Figures

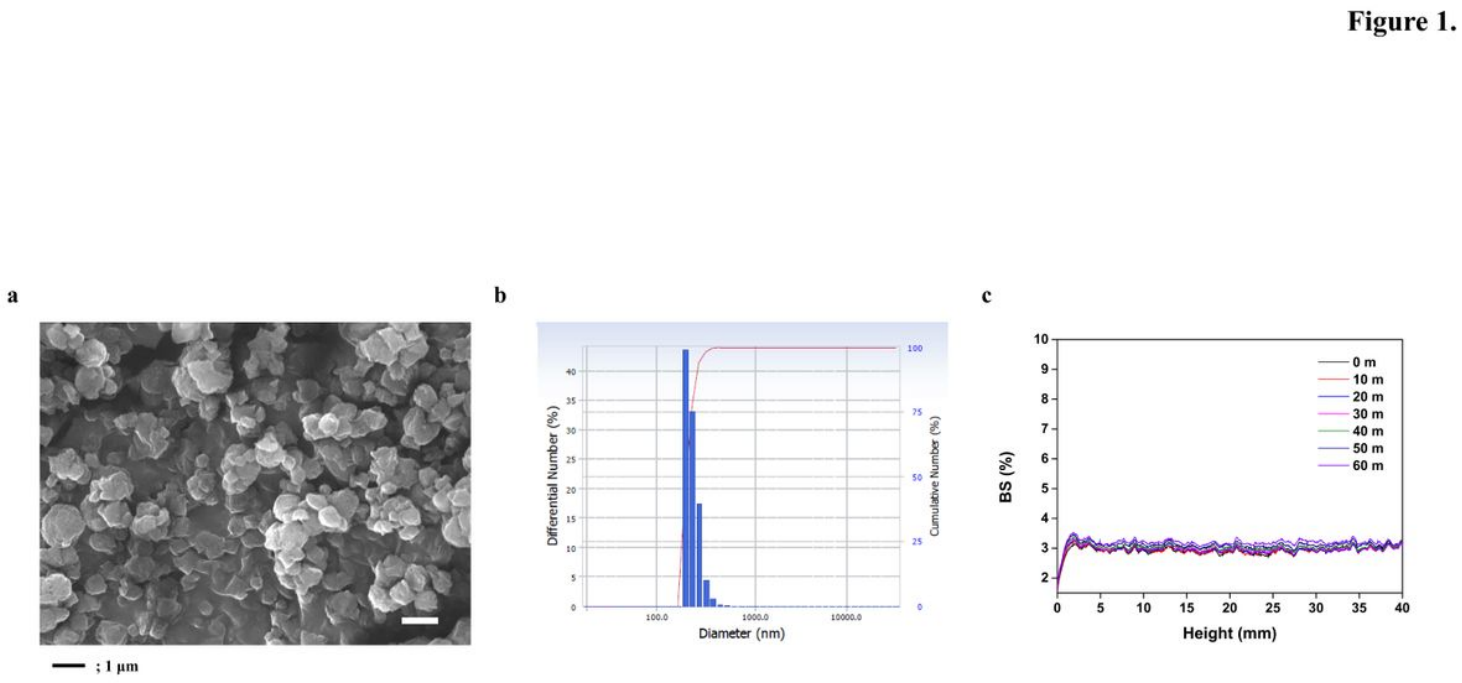

Figure 1

(a) FE-SEM image of PP microparticles. (b) DLS histogram showing the size distribution of PP microparticles. (c) Representative BS profiles and Turbiscan Stability Index (TSI) of PP microparticles. Scale bar 1 μm.

Figure 2.

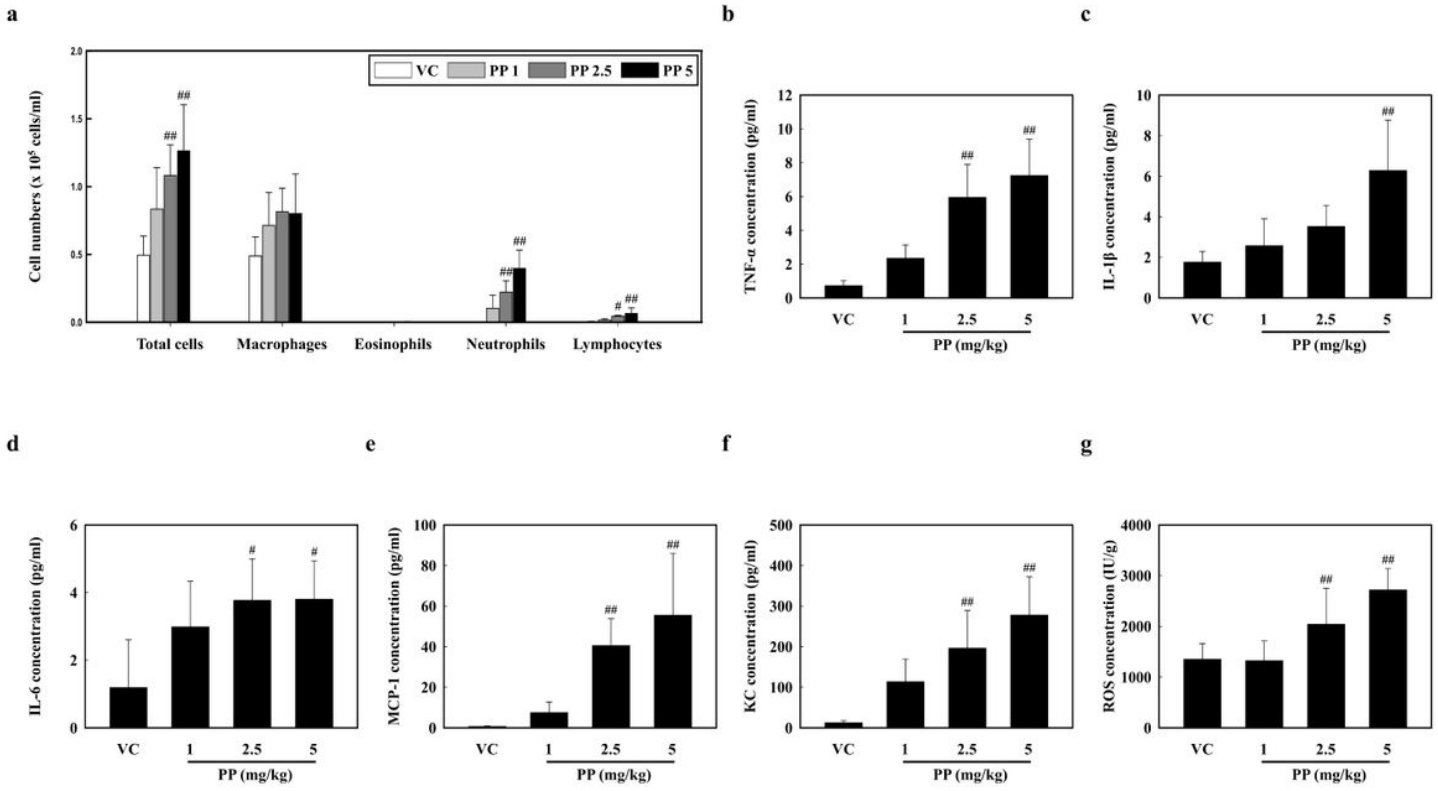

Figure 2

(a) Cellular changes in the BALF obtained from VC, PP 1 mg/kg (PP 1), PP 2.5 mg/kg (PP 2.5), and PP 5 mg/kg (PP 5) mice. Inflammatory cytokine and chemokine levels of BALF, including (b) TNF-α, (c) IL-1β, (d) IL-6, (e) MCP-1, and (f) KC. (g) ROS production in lung tissue. Data are presented as mean ± SD (n = 6 per group). $^{\#}P \leq 0.05$; $^{\#\#}P \leq 0.01$ vs. VC.

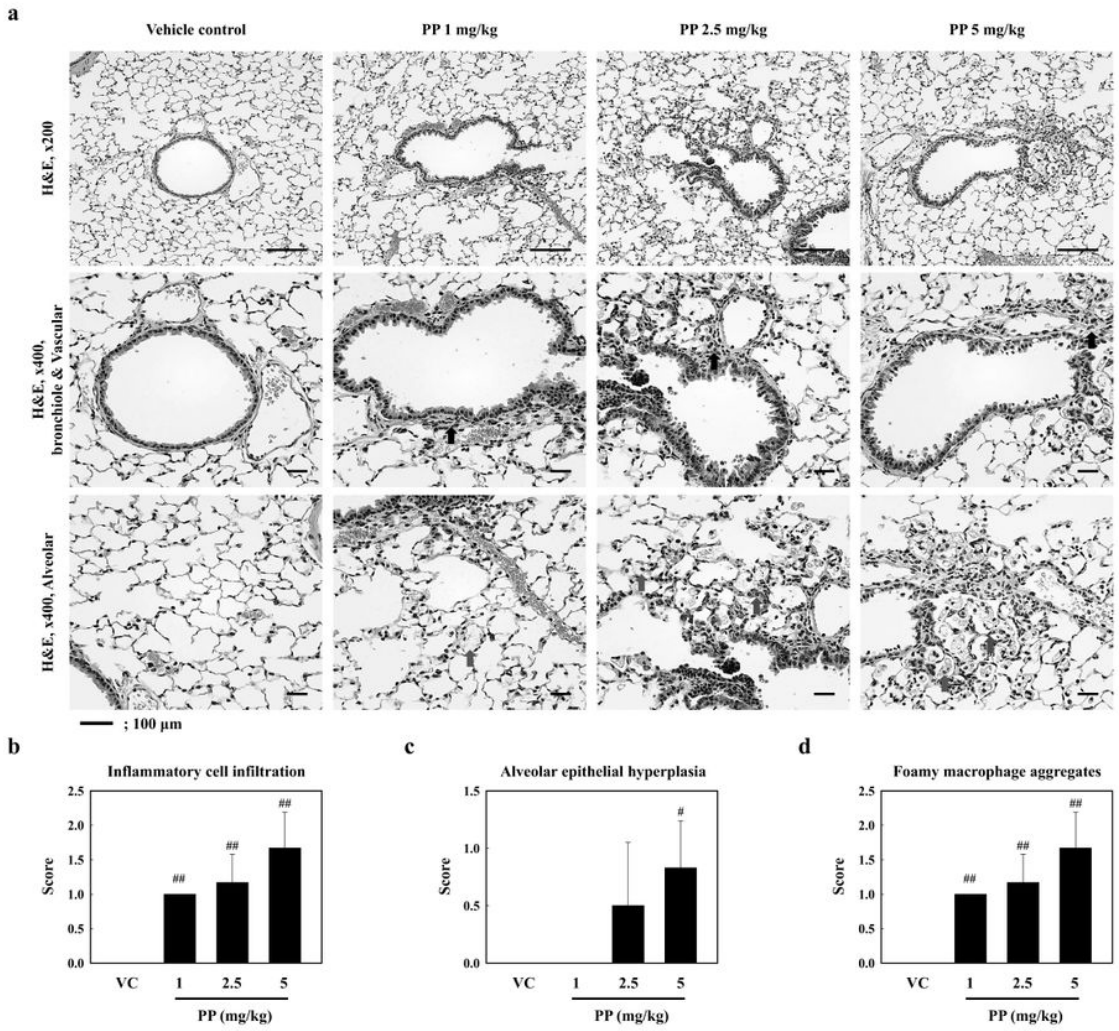

Figure 3

(a) Representative H&E-stained section of lung tissue. (b) Histological scoring of inflammatory cell infiltration, (c) alveolar epithelial hyperplasia, and (d) foamy macrophage aggregates. Black, red, and blue arrows indicate inflammatory cell infiltration in the perivascular/parenchymal layer, alveolar epithelial hyperplasia, and foamy macrophage aggregates, respectively. Data are presented as mean ± SD (n = 6 per group). $^{\#}P \leq 0.05$; $^{\#\#}P \leq 0.01$ vs. VC. Scale bar 100 µm.

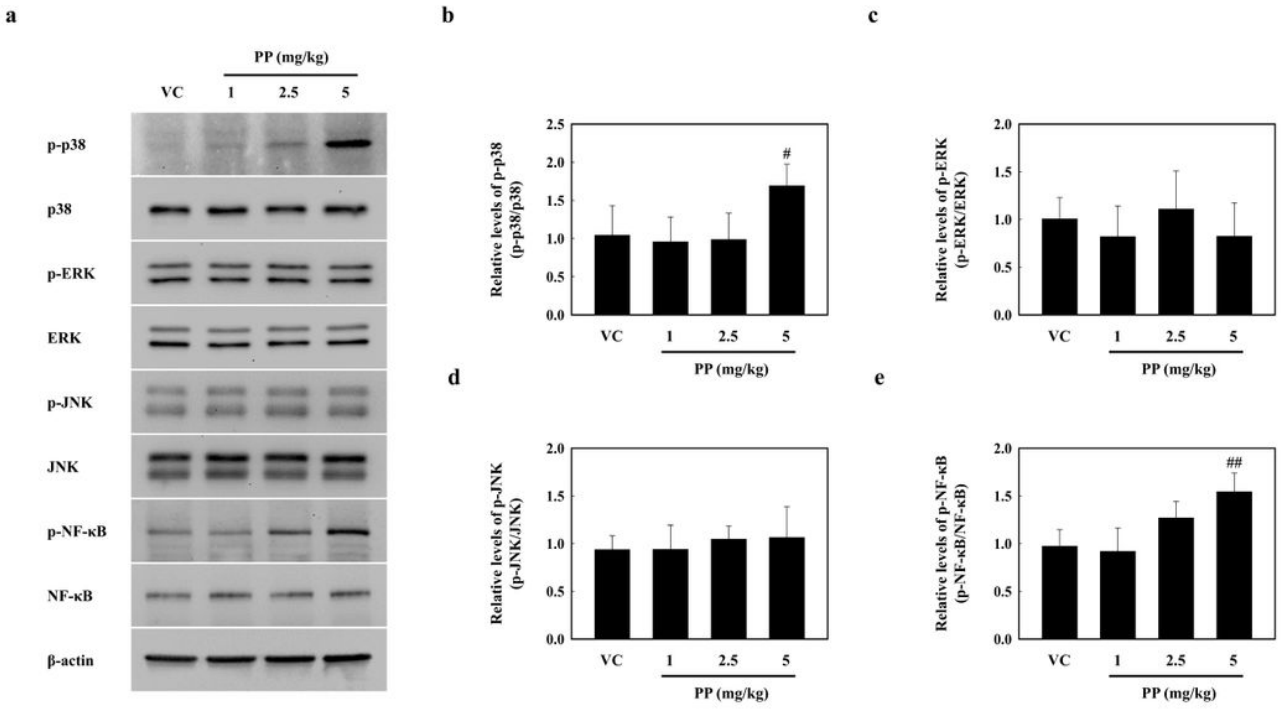

Figure 4

(a) Representative western blotting analysis of p-p38, p38, p-ERK, ERK, p-JNK, JNK, p-NF-κB, and NF-κB in lung tissue of PP-instilled mice. (b) Relative density analysis of p-p38 levels. Data were normalized against p38. (c) Relative density analysis of p-ERK levels. Data were normalized against ERK. (d) Relative density analysis of p-JNK levels. Data were normalized against JNK. (e) Relative density analysis of p-NF-κB levels. Data were normalized against NF-κB. Data are means ± SD (n = 6 per group). $^{\#}P \leq 0.05$; $^{\#\#}P \leq 0.01$ vs. VC.

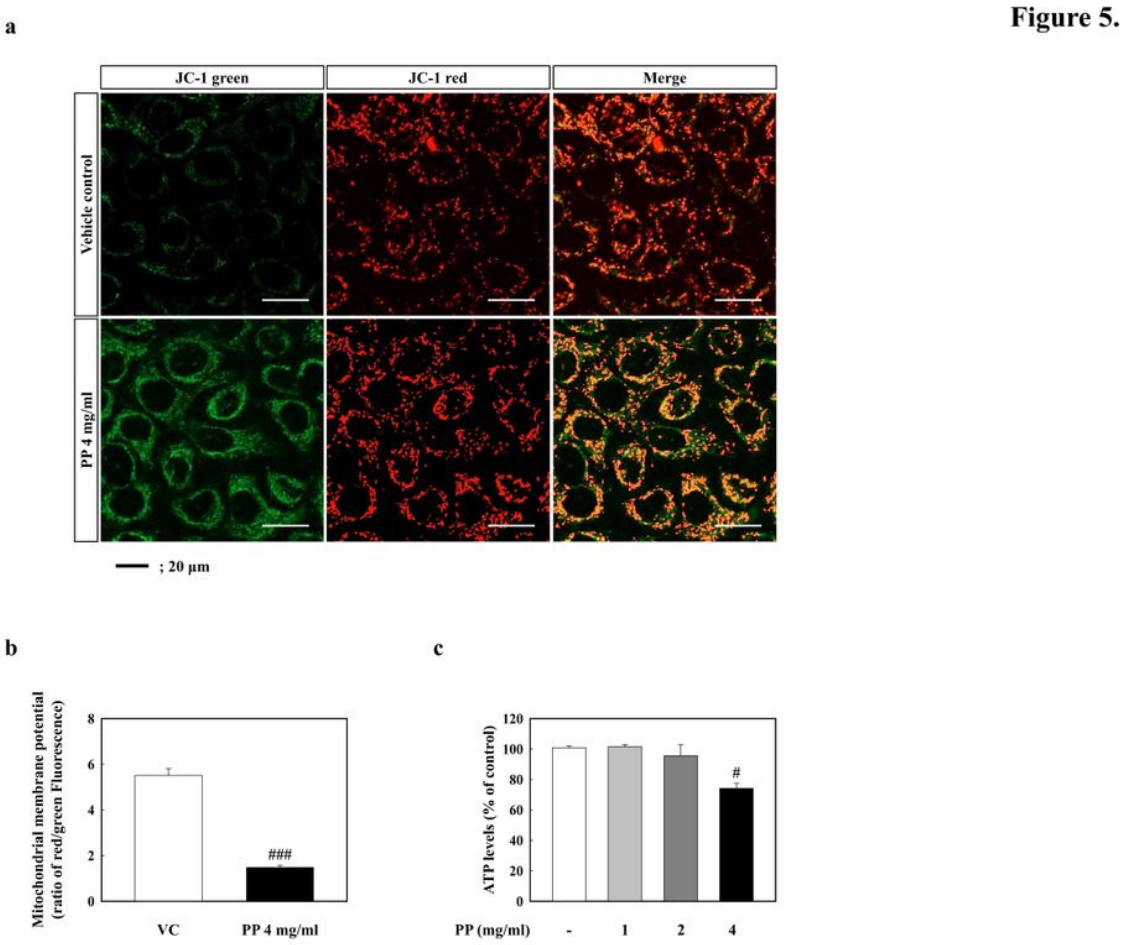

Figure 5

(a) Representative images with 2.5 μg/ml of JC-1 dye for 30 min. Red (568 nm) staining was in J-aggregate form, whereas green (488 nm) staining was in monomer form. (b) Mitochondrial depolarization is indicated by a decrease in the red/green fluorescence intensity ratio. (c) ATP assay was measured in cell lysates of PP-exposed A549 cells. Data are means ± SD (n = 3 per group). $^{\#}P \leq 0.05$; $^{\#\#\#}P \leq 0.001$ vs. VC. Scale bar 20 μm.

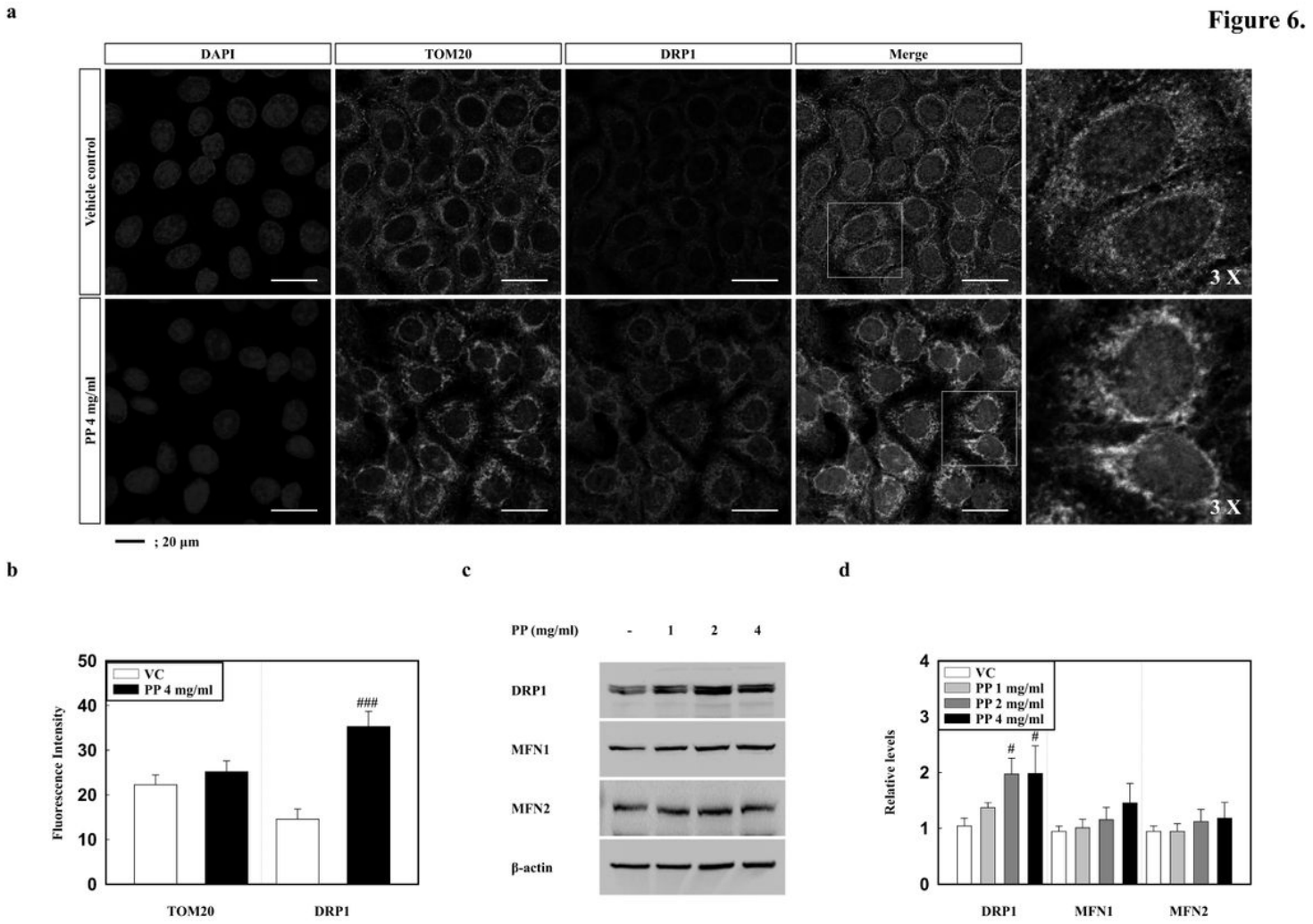

Figure 6

(a) Representative images of TOM20 (green: mitochondrial marker) and DRP1 (red) stained PP-exposed A549 cells. (b) Quantified staining intensities of TOM20 and DRP1. (c) Representative western blotting analysis for DRP1, MFN1, and MFN2 in cell lysates of PP-exposed A549 cells. (d) Relative density analysis of DRP1, MFN1, and MFN2. Data were normalized against β-actin. Data are means ± SD (n = 3 per group). $^{\#}P \leq 0.05$; $^{\#\#\#}P \leq 0.001$ vs. VC. Scale bar 20 μm.

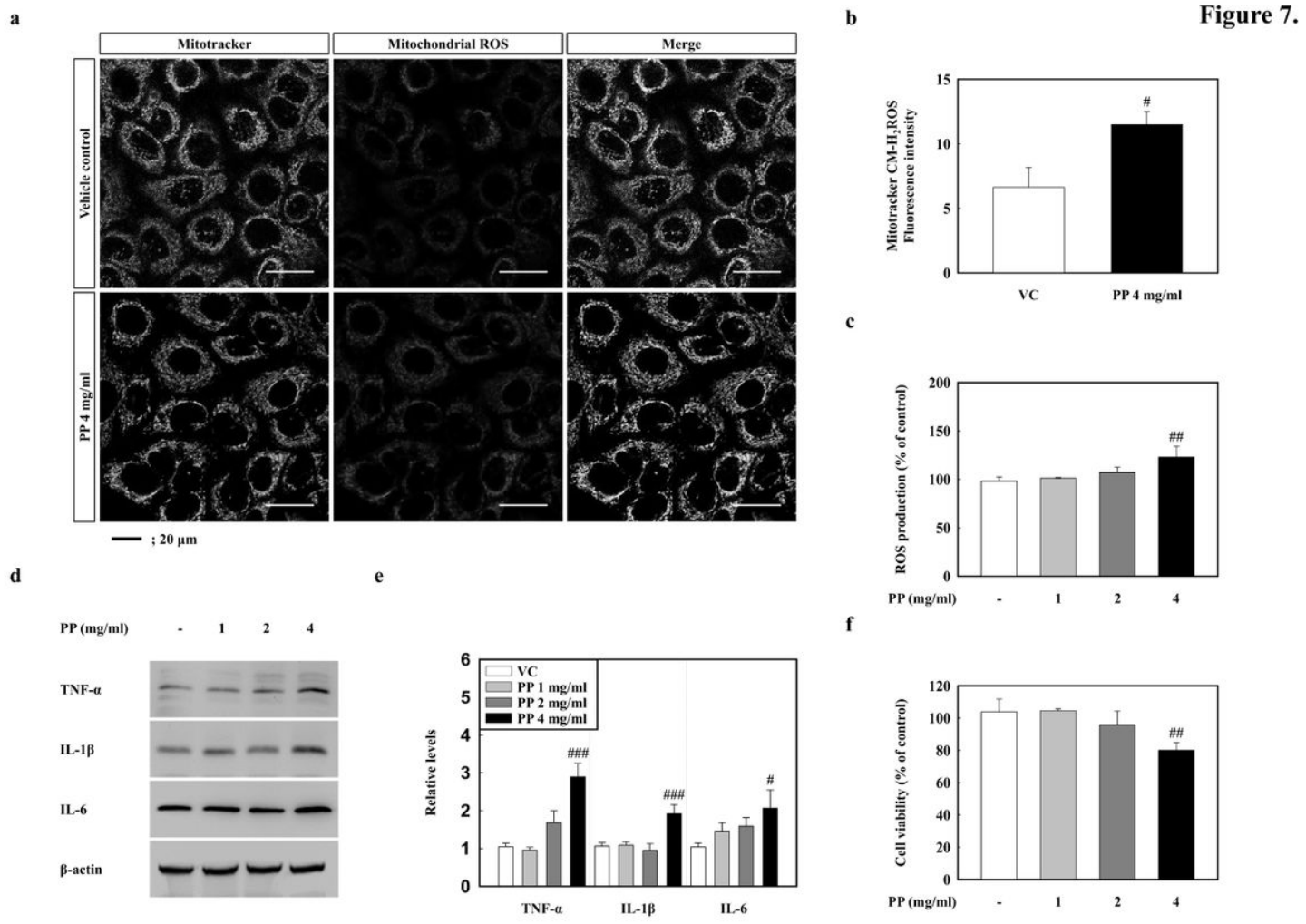

Figure 7

(a) Representative images of mitochondrial (green) and mitochondrial ROS (red) stained PP-exposed A549 cells that were treated with 200 nM for 30 min. (b) Quantified staining intensities for mitochondrial ROS. (c) Total ROS production in PP-exposed A549 cells. (d) Inflammatory cytokine levels of TNF-α, IL-1β, and IL-6 in cell lysate of PP-exposed A549 cells. (e) Relative density analysis of TNF-α, IL-1β, and IL-6. (f) Cell viability assessment by MTT assay. Data were normalized against β-actin. Data are means ± SD (n = 3 per group). $^{\#}P \leq 0.05$; $^{\#\#}P \leq 0.01$; $^{\#\#\#}P \leq 0.001$ vs. VC. Scale bar 20 μm.

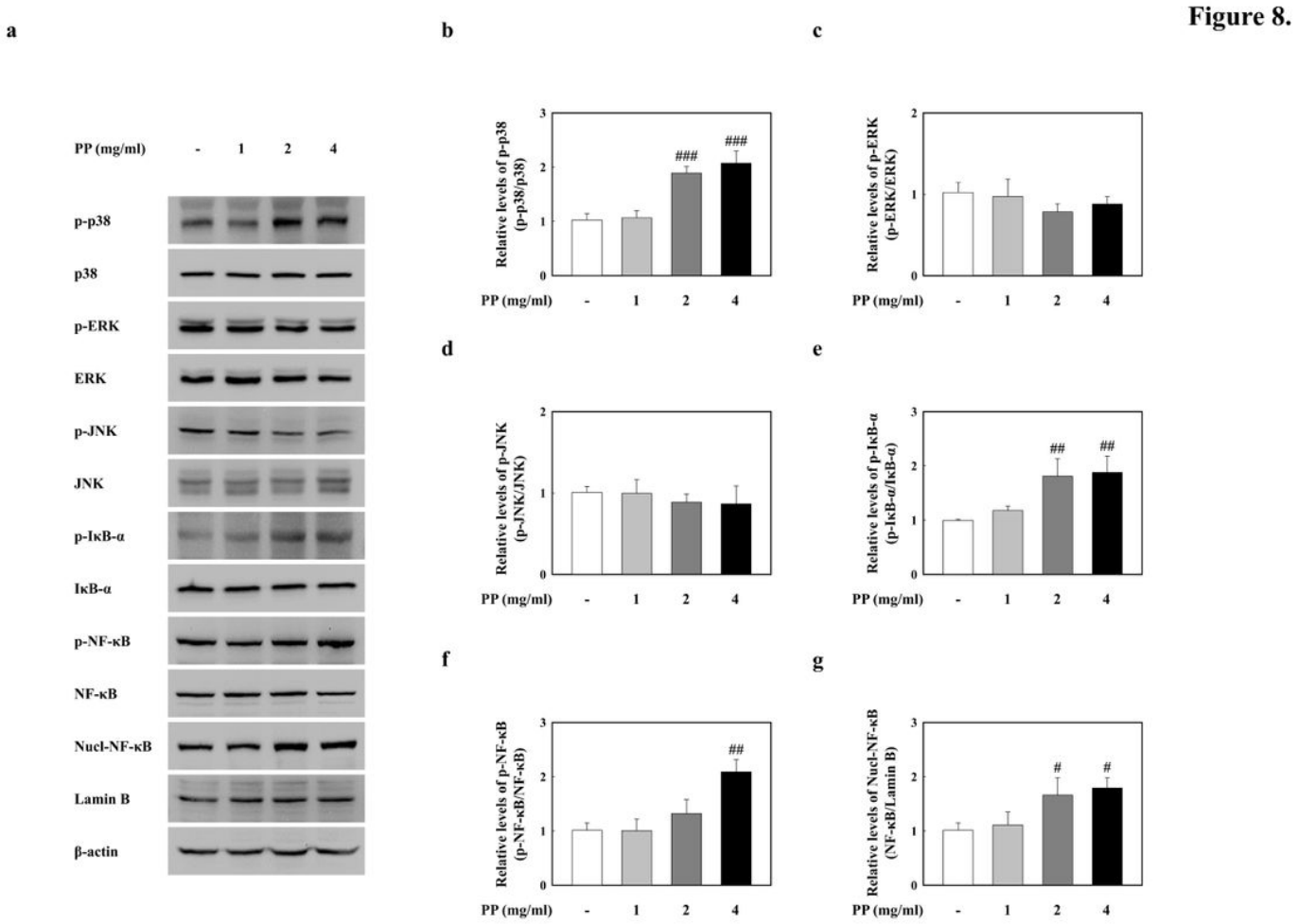

Figure 8

(a) Representative western blotting analysis of p-p38, p38, p-ERK, ERK, p-JNK, JNK, p-IκB-α, IκB-α, p-NF-κB, NF-κB, Nuclear-NF-κB, and Lamin B in PP-exposed A549 cells. (b) Relative density analysis of p-p38 levels. Data were normalized against p38. (c) Relative density analysis of p-ERK levels. Data were normalized against ERK. (d) Relative density analysis of p-JNK levels. Data were normalized against JNK. (e) Relative density analysis of p-IκB-α levels. Data were normalized against IκB-α. (f) The relative densities analysis of p-NF-κB levels. Data were normalized against NF-κB. (g) Relative density analysis of Nuclear-NF-κB. Data were normalized against Lamin B. Data are means ± SD (n = 3 per group). #P ≤ 0.05; ##P ≤ 0.01; ###P ≤ 0.001 vs. VC.

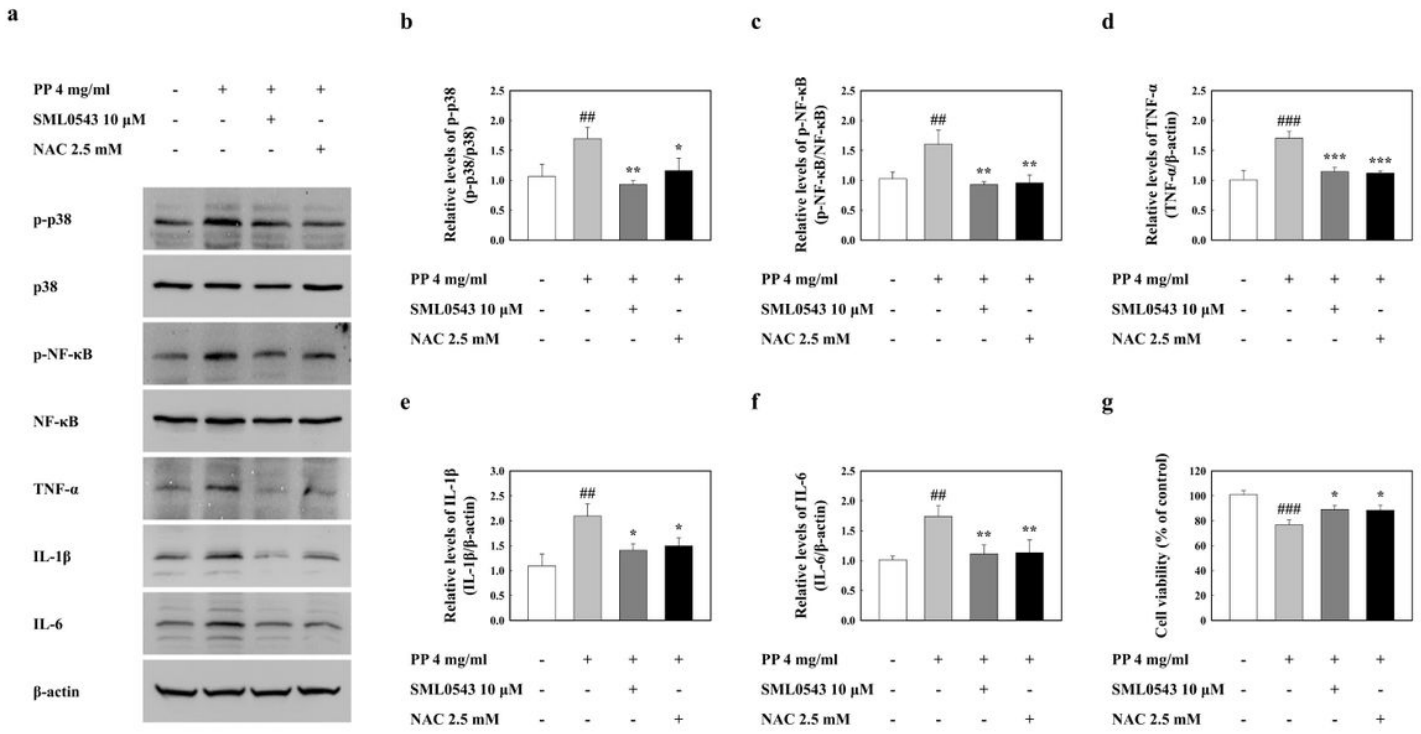

Figure 9

(a) Representative western blotting analysis of p-p38, p38, p-NF-κB, NF-κB, TNF-α, IL-1β, and IL-6 of PP-exposed A549 cells. (b) Relative density analysis of p-p38 levels. Data were normalized against p38. (c) Relative density analysis of p-NF-κB levels. Data were normalized against NF-κB. Relative density analysis of (d) TNF-α, (e) IL-1β, and (f) IL-6. Data were normalized against β-actin. (g) Cell viability assessment by MTT assay. Data are means ± SD (n = 3 per group). ##P ≤ 0.01; ###P ≤ 0.001 vs. VC. *P ≤ 0.05; **P ≤ 0.01; ***P ≤ 0.001 vs. PP.

Figure 10.

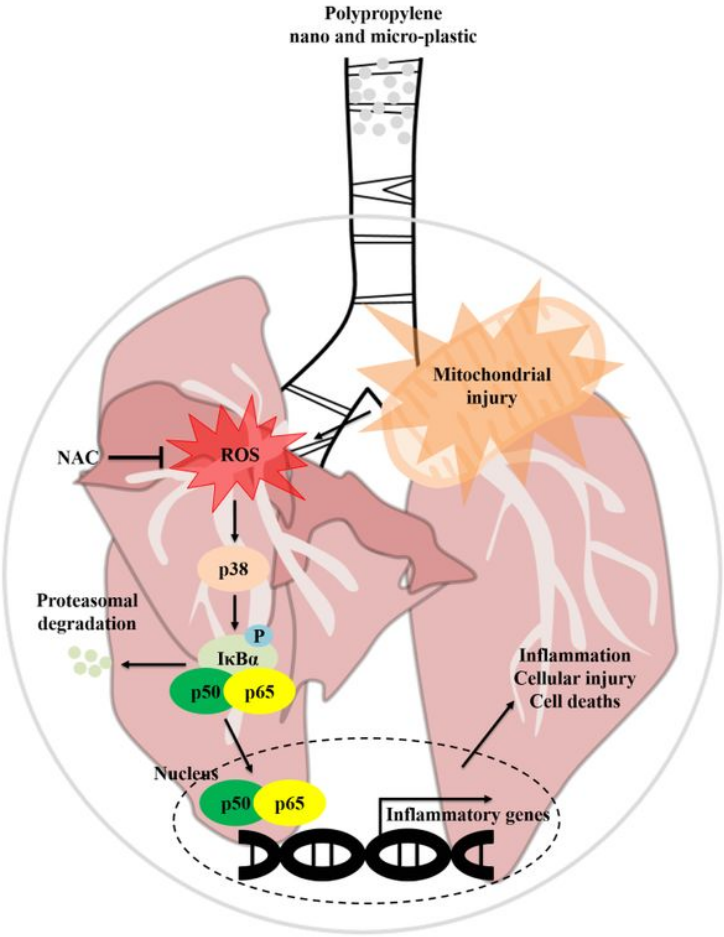

Figure 10

Pathway by which NF-κB signaling is a activated as a result of PP exposure in the lung

Supplementary Files

This is a list of supplementary files associated with this preprint. Click to download.

- Supplementary13.pdf
- SupplementaryFigureLegends.docx
- Westernblotrawdata.pdf